



Modeling of an High-Concentration Solar Reactor for Dry Methane Reforming

Jean-François Dufault^{1,*} , Emeric Désilets¹ , Nicolas Brissette¹, Nadi Braidy¹,
Luc G. Fréchette¹, and Mathieu Picard¹

¹Université de Sherbrooke, Canada

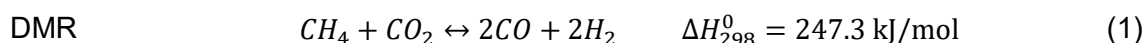
*Correspondance: Jean-François Dufault, Jean-Francois.Dufault@USherbrooke.ca

Abstract. Direct solar-powered reforming of methane has the potential to lower the CO₂ footprint of reforming and to harvest solar energy with high-efficiency [1]. Combined with bio-sourced feedstock and recycled CO₂ to perform dry methane reforming (DMR), this approach can highly decrease methane reforming environmental impact [2]. Using high solar concentration solar towers or parabolic dishes to provide the highly endothermal reaction heat required for DMR, it is possible to reach the temperatures of conventional reformers, ranging from 800°C up to 900°C. At this temperature, radiation losses are such that high solar concentrations approaching 1000x are required to reach high thermal efficiency, making heat flux management highly challenging. Previous work from Université de Sherbrooke experimentally shown the potential for such reactors to operate under high heat flux [3],[4]. The current work presents the modeling approach used to design these reactors and increase the heat flux within the absorption surface, while maintaining reasonable temperature drop within the reactor. Dimensional analysis if first assess that no diffusion limitation occurs within the reactor and the system can be simulated as a plug flow reactor with porous catalyst. Using DMR and RWGS kinetics from literature with 2D modeling in COMSOL Multiphysics, temperature and reaction rates along the reactor are evaluated showing consistency with experimental values. Parametrical analysis shows that optimal catalyst channels width appears to be equal or under 0.5 mm. Finally, it is demonstrated that optimal conversion occurs when around 1/3 of the catalytic bed is covered with metallic conductive fins. Over this value, increased conductivity gains are overpassed by the lowering of catalyst volume within the conduction chamber.

Keywords: Solar Fuels, Dry Methane Reforming, Micro Reactors

1. Introduction

Dry methane reforming (DMR) is a process by which CO₂ and CH₄ reacts together to produce synthesis gas (eq. (1)), a valuable feedstock to produce chemicals, such as methanol or other carbonaceous compounds through Fischer-Tropsch process. To maintain sufficient reaction rate, this highly endothermal process ($\Delta H=247.3$ kJ/mol), must operate under high temperatures ranging from 800 °C to 900 °C within a catalyst packed. In conventional SMR reformers, for example, this energy is supplied by the combustion of a portion of the natural gas feedstock, leading to additional CO₂ emissions and natural resources consumption.



Solar reforming aims at reducing the DMR syngas production footprint by replacing the heat input by concentrated solar power. To reach temperatures over 800 °C, solar rays are

concentrated using optical systems such as solar towers and parabolic troughs. At the focal point of concentrators, heat flux reaches from 500 to 1000 times the solar irradiance at sea level, meaning 500 to 1000 kW/m². Although such heat flux is required to encompass the radiation losses at operation temperatures, considerable efforts must be made to conduct energy to the reaction zone.

Solar receivers for methane reforming appear in two main categories in literature, namely open and close receivers [5]. Open receivers characterize using a heat-resistant window to let the sunlight enter the receiver's cavity and directly hit the catalytic zone. The benefit of this system is to directly supply the reaction zone, without the need for intermediary conduction between the absorption and the reaction points. Potential challenges encountered with these systems are the sealing and potential cooling of the windows as well as its capacity to sustain reforming operation pressure ranging from 2 to 30 bars in conventional SMR reformers. Since solar towers focal point can reach several square meters, the scalability of such windows might also be challenging while not impossible. Closed receivers, on the other hand, use a solar absorptive surface to harvest energy while heat is conducted to the reaction zone within the reactor's structure and catalyst. This configuration has the benefit of simplicity of sealing, pressure resistance, and scalability, but implies high thermal gradient within the structure at such heat flux. Indeed, roughly 50 °C per mm of structure will be lost to conduct a 1000 kW/m² heat flux in Inconel 625 at operation temperature, meaning that the absorption surface must be thin to avoid excessive surface temperature and radiation losses. Such systems have been shown to be highly effective in the past for parabolic dishes by the PNNL [6]. Furthermore, the round configuration of the PNNL's receiver, coupled with radial flow, perpendicular the absorption surface makes this reactor well adapted to parabolic dishes, but their adaptation to solar towers remains unexplored.

Previous work from the Université de Sherbrooke (UdS) shown promising results and high scalability potential for use on solar tower and even radiative electrical elements [3], [4], [7], [8]. The approach inspired by micro-manufacturing uses a series of high-density micro-chamber operating in parallel to cover the surface of a receiver. Using micro-channels, allows to operate the reactor at high pressure while maintaining a low absorption surface thickness, which is helpful to maintain low absorptive surface temperature. These reactors have shown to operate at high heat flux and methane conversion under simulated and real environment. Parallelizing of the system has also found to be feasible, but management of the incoming heat flux remains challenging, while necessary for high efficiency.

This study shows the modeling process of these reactors to provide better understanding of the current architecture for eventual optimisation. First, the reaction zone is detailed, and the general system's architecture are detailed. Dimensional analysis is used to validate assumption used to model the reaction domain. The DMR reaction kinetics is then evaluated and reaction rates used entered into a COMSOL parametrical study to evaluate their effect on the reactor's conversion. Results are finally analysed to emerge general rules for the design of such reactors.

2. Reactor's architecture

The studied reactors are made of 3D-printed Inconel 625 equipped with a CO₂ + CH₄ inlet, an optional water inlet and a syngas exhaust (Figure 1-a). During their descent to the catalytic bed, reagents are preheated by the hot products exhausting within a s-shaped counterflow heat exchanger (Figure 1-b).

Reagents are then heated by the outgoing products until they get into a second plenum designed to spread flow uniformly into micro-channels Figure 1-c. These micro-channels then bring the flow near the absorption zone where it crosses filters and then several channels packed with catalyst. These vertical millimetre-scale fins, parallel to the reactor's solar absorption, also serve to transport heat from the absorption surface through the reaction bed. Nickel-

based catalyst crushed in particles is placed between the fins to accelerate DMR reaction. As the reaction occurs, reagents transform to product until it gets to the top of the catalytic bed where other filters are placed to maintain catalyst. Flow then passes through the exhaust plenum to enters the hot side of the heat exchanger and finally exhaust the reactor. This architecture allows the use of a 2D model and axial periodicity to reduce computing time (Figure 1-d-e).

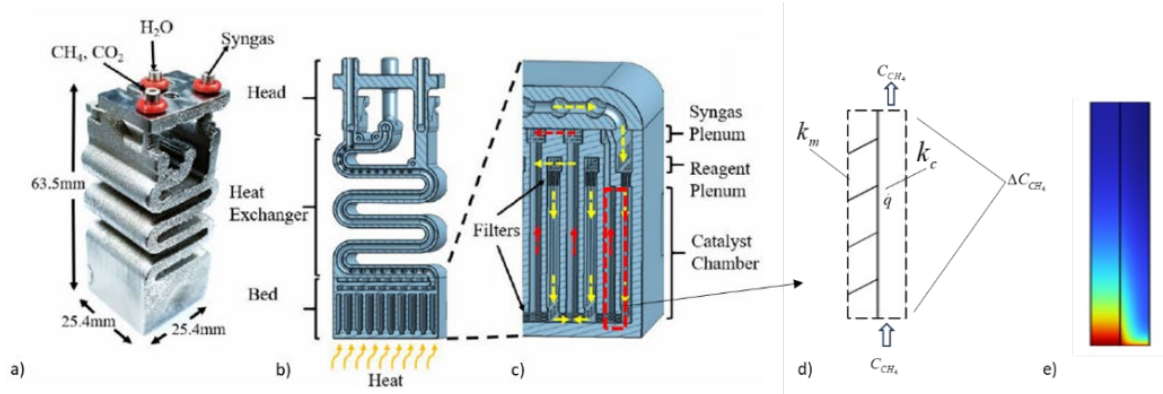


Figure 1. a) and b) Reactor's architecture [9], c) close view of the catalytic bed and d) domain used in the COMSOL model and e) typical 2d temperature profile evaluated with COMSOL.

3. Modeling approach

3.1 Numerical model

The current system comprises features and phenomenon ranging from the atomic to the centimeter scale. To properly account for each of these phenomena without increasing computation time, analysis of the dominant phenomena have been performed and reaction domain is simplified (Figure 2). Indeed, low Reynold's number within the catalyst allow to treat flows as simple Darcy flow and other numbers such as Mears, Weis-Prater show that no heat or mass diffusion limitation occurs within or around the catalyst pellets. Dam Kohler number also proved the heat of reaction to be much higher than the sensible energy carried by the reactive, allowing to neglect heating of the downward incoming reagents within the conductive fins (Figure 2). Fully developed plug flow is considered through all the domain since the catalyst bed's length is much longer than its width.

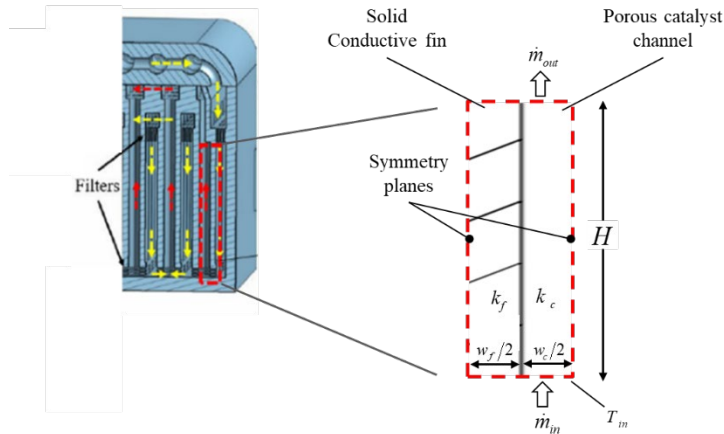
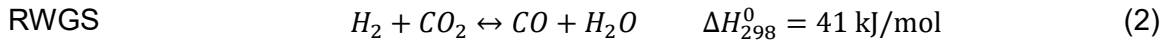


Figure 2. Modeled region of the reactor comprising an isothermal entrance, two symmetry planes and an adiabatic exhaust

Catalytic zone geometry is described by the length of the channels and fins H , as well as the catalyst bed and fins width w_c and w_f respectively. Uniform temperature at the bottom of the fins and catalyst channels and perfectly insulated fins top are used as boundary conditions. COMSOL Multiphysics software is used to solve the model. Analyses are performed considering the thermodynamics, chemistry, transport of concentrated species in porous media, heat transfer in porous media and free and porous media flow simultaneously. Reaction rates used are directly included in the COMSOL chemistry module and described at section 3.1. The developed model is then used to perform parametrical analysis to establish the impact of the catalyst thermal conductivity k_c , catalyst channels width w_c , as well as the effect of the ratio between the fins, and catalyst channels widths $w_c : w_f$. Optimal balance is then expected to change with the catalyst and fins thermal conductivity k_c and k_f as well as the catalyst kinetics and operation conditions such as the entrance temperature T_{in} , entrance pressure P_{in} , $CO_2:CH_4$ ratio and exhaust methane conversion α_{CH_4} .

3.2 Kinetics

Several parallel reactions occur during dry reforming of methane with DMR and reverse water gas shift (RWGS) reaction (eq. (2)) being the main components of heat consumption and CO production [10], [11], [12].



Although other reactions might have an impact on the conversion, only these two are here considered as they shown good results using this representation. The DMR and shift rate equations r_1 (eq.(3)) and r_2 (eq.(4)) and constants used in the present work are obtained from Paripatyadar [13] derive from a Langmuir-Hinshelwood type mechanism of a 0.5%wt Rh/Al₂O₃ catalyst. Kinetic data obtained from former work were validated through further experiments in both a pellet string reactor and a pilot unit solar receiver [14]. In the current study, the kinetics depicted an adequate representation of heat flux, temperature, and partial pressure dependencies in the current modelling of the reaction zone.

$$r_1 = \frac{k_1 K_{CO_2,1} K_{CH_4,1} P_{CH_4} P_{CO_2}}{1 + K_{CO_2,1} P_{CO_2} + K_{CH_4,1} P_{CH_4}} \left(1 - \frac{(P_{CO} P_{H_2})^2}{K_{P_1} (P_{CH_4} P_{CO_2})} \right) \quad (3)$$

$$r_2 = \frac{k_2 K_{CO_2,2} K_{H_2,2} P_{CO_2} P_{H_2}}{1 + K_{CO_2,2} P_{CO_2} + K_{H_2,2} P_{H_2}} \left(1 - \frac{(P_{CO} P_{H_2O})^2}{K_{P_2} (P_{CO_2} P_{H_2})} \right) \quad (4)$$

The latter consider an Arrhenius driven reaction rate constants, k_j , as well as Van't Hoff driven equilibrium constants, $K_{p,j}$, and a fitted model for adsorption constants, $K_{i,j}$ (eq. (5)-(6)).

$$K_j = K_{0,j} \exp\left(-\frac{\Delta H_j}{RT}\right) \quad (5)$$

$$k_j = k_{0,j} \exp\left(-\frac{E_{a,j}}{RT}\right) \quad (6)$$

$$k_1 = 1.29 \times 10^6 \exp\left(\frac{-102065}{RT}\right) \quad (7)$$

$$K_{CO_2,2} = 0.5771 \exp\left(\frac{9262}{RT}\right) \quad (8)$$

$$k_2 = 0.35 \times 10^6 \exp\left(\frac{-81030}{RT}\right) \quad (9)$$

$$K_{H_2,2} = 1.494 \exp\left(\frac{6025}{RT}\right) \quad (10)$$

$$K_{CO_2,1} = 2.61 \times 10^{-2} \exp\left(\frac{37641}{RT}\right) \quad (11)$$

$$K_{p_1} = 6.78 \times 10^{14} \exp\left(\frac{-259660}{RT}\right) \quad (12)$$

$$K_{CH_4,1} = 2.60 \times 10^{-2} \exp\left(\frac{40684}{RT}\right) \quad (13)$$

$$K_{p_2} = 56.4971 \exp\left(\frac{-36580}{RT}\right) \quad (14)$$

Which are specifically expressed:

These reactions are directly integrated within the COMSOL Multiphysics Chemistry module, and the transport and chemical properties of each species are calculated within the Thermodynamics module. The specific molar reaction rates, r_i (eq. (15)), are described within the software using summation of the kinetic data from previously mentioned literature:

$$r_i = \sum_{j=1}^m \nu_{ij} r_j \quad (15)$$

4. Results and analysis

A first design point was run and is considered as the baseline for the rest of the study. This baseline uses the same dimensions as the reactor tested by Francoeur et al. which has a bed length H , a fin width w_{fin} and catalyst channel width w_{cat} of 10 mm, 1 mm and 1 mm respectively. Figure 3 shows the species molar fractions, reaction rates and temperature profile along the catalyst channels while operating at 800°C and a GHSV of 35 000 h⁻¹. As expected with packed bed reactors, high reaction rates occur at the reactor entrance and quickly reduce as reagent concentrations diminish. This behaviour provokes a quick temperature drop within the first millimeters of reactor as the reaction consumes high quantity of energy. The temperature profiles then stabilizes as less heat flux passes through the conductive fins. It also must be mentioned that the high temperature gradient between the entrance and exhaust of the channels is consistent with results obtained by Francoeur et al. and molar compositions coincide with results from [15]. It indeed appears that RWGS reaction gets important as soon as the hydrogen content increases, explaining presence of water within the products and higher selectivity toward CO. This result implies that higher CO₂ conversion must be expected using such catalyst and that higher CO₂:CH₄ ratio should be used to increase CH₄ conversion for a given temperature.

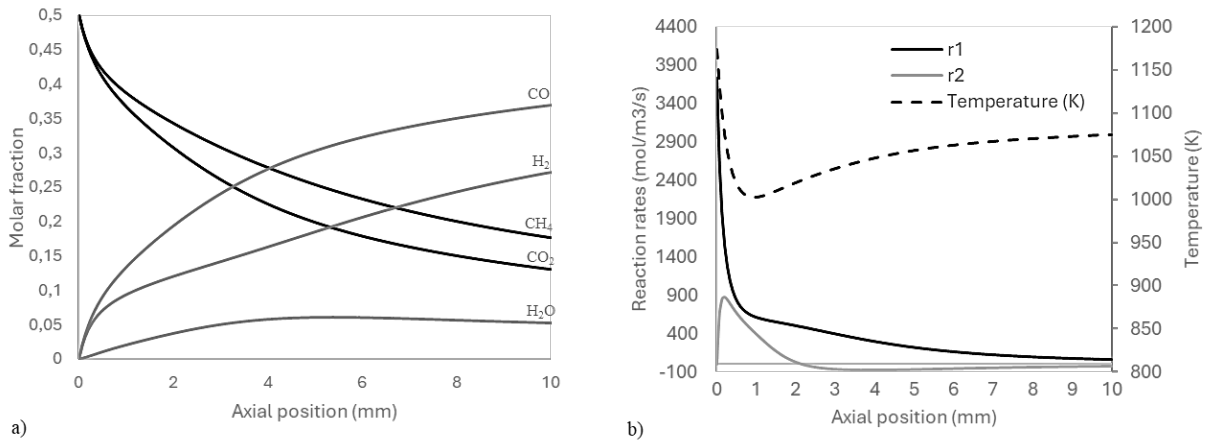


Figure 3. Profiles along the catalytic chamber for, a) molar fraction of each species, b) DMR and RWGS reaction rate and temperature

Parametric COMSOL analysis was also performed to assess the effect of catalyst pockets and fins width w_{cat} and w_{fin} , and respective conductivities k_{cat} and k_{fin} . Figure 4-a shows analysis where the width ratio between catalyst and fins ($w_{cat} : w_{fin}$) was maintained constant to 1 and while varying catalyst conductivity and catalyst channels width. For low catalyst conductivity, results show quick reduction of the methane conversion when w_{cat} reduces. This result

is mainly caused by transversal temperature drop within the catalyst as channels get bigger, which also explain why the effect vanishes as the conductivity increases. Another interesting point is that catalyst conductivity only causes small variation of conversion for low catalyst channel width. This can be explained by the small contribution of the catalyst conductivity on the vertical conduction when much smaller than fins conductivity (eq. (16)).

$$k_{eff,y} = \frac{k_{cat}w_{cat} + k_{fin}w_{fin}}{w_{cat} + w_{fin}} \quad (16)$$

Consequently, appreciable conversion gain only occurs when thermal conductivity of the catalyst reaches the same order of magnitude as the fins, which is hardly obtained for a porous catalyst. Finally, results of Figure 3-a shows that a conversion plateau happens for catalyst pocket width lower than 0.5 mm, which approach the current metal 3D printing limits.

Effect of catalyst-fin width ratio is observed on Figure 4-b. For the given operation conditions, conversion increase is observed when catalyst proportion passes from 0.5 to 1.5. However, the improvement becomes negligible beyond a ratio of 2, with the curves for $w_{cat}/w_{fin}=1.5$ and 2 being nearly indistinguishable in the high-performance region (near $w_{cat}=0$). This indicates a saturation point where further increasing the catalyst channel width relative to the fin width no longer yields a significant gain in conversion. At this point gains of having higher catalyst content gets compromised by the reduction of vertical conductivity coming with lower metal content. Since no reaction occurs within the metallic fins, compromise between conversion and total heat consumption (and heat flux) must be made.

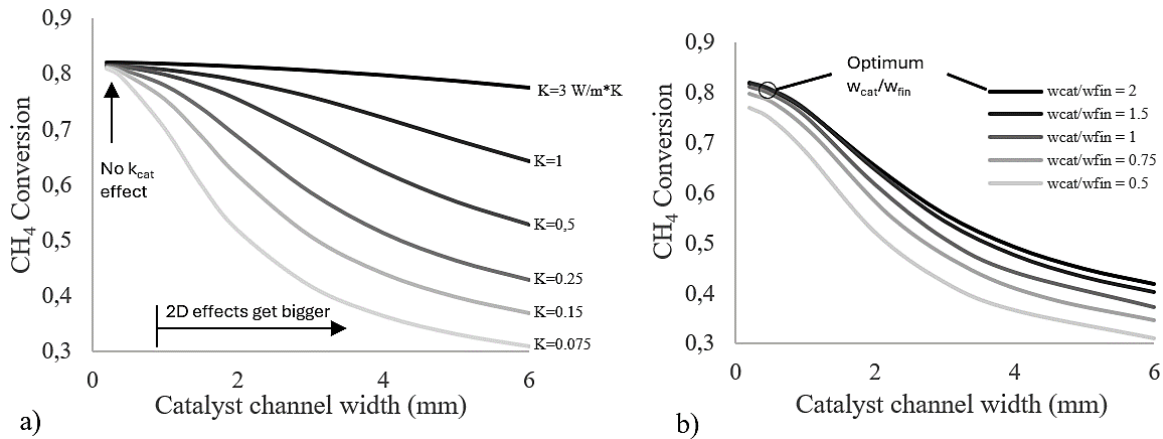


Figure 4. Conversion over the maximum achievable isothermal conversion with catalyst bed width

5. Conclusion

Dry methane reforming using concentrated solar power is a promising way for both CO₂ revalorization and renewable energy production. To reach economical viability, high thermal efficiency and reagent conversion must be achieved, meaning that high heat flux and reaction rates must be processed within the reactor. Experimental work from the Université de Sherbrooke experimentally shown that high performance is reachable using 3D printed micro reactors. This document presents the modeling efforts made to understand the parameters governing conversion and heat use within the reactor tested by Francoeur et al. for future optimization. Dimensional analysis first confirmed the low Reynolds number flow and high transport phenomena inherent to miniaturized systems as well as the validity of simplified bed description of the homogeneous flow in porous catalyst. The Dam Köhler II number also revealed weak influence of the advection on the energy transport, making the description of the reaction

zone as a simple juxtaposition of a metallic fin and plug flow catalytic channel possible. Langmuir Hinshelwood kinetic description of the DMR and RWGS reaction was used to describe rates of species consumption and creation within the catalyst. 2

2D COMSOL Multiphysics modeling of the reaction zone using the previously mentioned hypothesis shown good fidelity with literature and experimental value previously obtained. Values obtained at atmospheric pressure for an operation point of 800°C and a GHSV of 65 000 h⁻¹ and a CO₂:CH₄ ratio of 1 shows high energy consumption within the first millimeters of reactor which also coincide with the high temperature drop present at the entrance. High attention to the low exhaust temperature must be given in future works as these conditions might accelerate catalyst coking.

Parametrical analysis ran to assess the effect of the reaction zone geometry and catalyst conductivity shows that maximum conversion comes for low catalytic bed width, where transversal conduction is sufficient to supply heat to the reaction without influencing rates of species consumption. At that point, 2D description can simplify to an axial 1D model, for which thermal conductivity is pondered with the respective volumes and conductivity of catalyst and conductive fins within the reaction zone. For the current reaction, this point for channels having less than 0.5 mm, which is close to the metal 3D printing limits. In this region, appreciable conversion gain was obtained only when catalyst conductivity gets close to the fins one.

The ratio between catalyst channels and conductive fins width also shown an optimal value around $w_{cat} : w_{fin} = 2$, with the impact being slightly dependent on the channel width itself. Future work will focus on the evaluation of the system's thermal efficiency as well as the geometric optimization of the catalytic zone.

Notation

Symbols

A_e	Frequency factor	
C_i	Concentration of <i>i</i> th species	mol/m ³
D_{AB}	Mass diffusivity of species <i>A</i> in <i>B</i>	m ² /s
E_a	Activation energy	J/mol
GHSV	Gas hourly space velocity	h ⁻¹
h	Heat convection coefficient	W/m ² *K
k_{cat}	Catalyst thermal conductivity	W/m ² *K
k_j	Reaction rate constant in <i>j</i> th reaction	
$K_{p,1}$	Equilibrium constant for DRM	Pa ²
$K_{p,2}$	Equilibrium constant of <i>j</i> th reaction	-
$K_{i,j}$	Adsorption constant of <i>i</i> th species in <i>j</i> th reaction	-
k_f	Fins thermal conductivity	W/m ² *K
L_b	Catalytic bed length	m
L_c	Characteristic length	m
MR_T	Thermal Mears number	-
MR_M	Mass Mears number	-
n	Reaction order	-
P_i	Partial pressure of species <i>i</i>	Pa
P_{in}	Catalyst bed entrance pressure	Pa
q_{abs}''	Absorbed heat flux	W/m ²
r'	Reaction rate	mol/s/m ³
R_c	Channel radius	-
R_p	Pellets Radius	m
R_g	Universal gas constant (8.31)	J/mol*K
Re_D	Reynolds number base on the diameter	-
T_{in}	Catalyst bed entrance temperature	K

Greek letters

α_{CH_4}	Methane conversion	-
ν_{ij}	Stoichiometric coefficient of <i>i</i> th species in <i>j</i> th reaction	-
η_{th}	Thermal efficiency	-
ϕ_p	Pellets porosity	-
σ_c	Constriction factor	-
ρ_b	Bulk catalyst density	Kg/m ³
$\tilde{\tau}$	Tortuosity	-

V	Fluid velocity	m/s
w_{cat}	Width of the catalyst bed	m
w_f	Width of the metallic fins	m

Data availability statement

All data, models, and code generated or used during the study appear in the published article

Author contributions

Jean-François Dufault: Conceptualization, Data curation, Formal analysis, Funding acquisition, Investigation, Methodology, Project administration, Software, Resources, Supervision, Validation, Visualization, Writing – Original Draft, Writing – review & editing. **Emeric Désilets:** Data curation, Investigation, Resources, Writing – review & editing. **Nicolas Brissette:** Funding acquisition, Writing – review & editing. **Paul Camus:** Resources. **Nadi Braidy:** Methodology, Supervision, Writing – review & editing. **Luc G. Fréchette:** Conceptualization, Funding acquisition, Supervision, Validation, Writing – review & editing. **Mathieu Picard:** Conceptualization, Supervision, Validation, Writing – review & editing

Competing interests

The authors declare that they have no competing interests.

Acknowledgement

Funded by the European Union under the Horizon Europe Framework Programme (Project name: SOLARX; grant number: 101084158). Views and opinions expressed are however those of the author(s) only and do not necessarily reflect those of the European Union or the European Climate, Infrastructure and Environment Executive Agency (CINEA). Neither the European Union nor the granting authority can be held responsible for them. The project is also supported by the NSERC, FRQNT and MITACS.

References

- [1] C. Agrafiotis, H. von Storch, M. Roeb, et C. Sattler, « Solar thermal reforming of methane feedstocks for hydrogen and syngas production—A review », *Renewable and Sustainable Energy Reviews*, vol. 29, p. 656-682, janv. 2014, doi: [10.1016/j.rser.2013.08.050](https://doi.org/10.1016/j.rser.2013.08.050).
- [2] B. R. De Vasconcelos et J.-M. Lavoie, « Is dry reforming the solution to reduce natural gas carbon footprint? », *Int. J. EQ*, vol. 3, n° 1, p. 44-56, janv. 2018, doi: [10.2495/EQ-V3-N1-44-56](https://doi.org/10.2495/EQ-V3-N1-44-56).
- [3] D. Francoeur et al., « Solar Methane Reforming Microreactor Proof-Of-Concept With A 2X2 Array on a Full-Scale Dish », *SolarPACES Conference Proceedings*, vol. 1, janv. 2024, doi: [10.52825/solarpaces.v1i.886](https://doi.org/10.52825/solarpaces.v1i.886).
- [4] P. Camus, J.-F. Dufault, D. Mehanovic, N. Braidy, L. G. Fréchette, et M. Picard, « Testing of a 3D-Printed Solar Micro-Reactor for Hydrogen Production via Natural Gas Reforming », in *Power MEMS 2019*, Daytona Beach, FL, USA, déc. 2019, p. 4.
- [5] E. J. Sheu, E. M. A. Mokheimer, et A. F. Ghoniem, « A review of solar methane reforming systems », *International Journal of Hydrogen Energy*, vol. 40, n° 38, p. 12929-12955, oct. 2015, doi: [10.1016/j.ijhydene.2015.08.005](https://doi.org/10.1016/j.ijhydene.2015.08.005).
- [6] R. Zheng et al., « Integrated Solar Thermochemical Reaction System for Steam Methane Reforming », *Energy Procedia*, vol. 69, p. 1192-1200, mai 2015, doi: [10.1016/j.egypro.2015.03.204](https://doi.org/10.1016/j.egypro.2015.03.204).

- [7] J.-F. Peloquin et al., « Electrified steam methane reforming microreactor », *International Journal of Hydrogen Energy*, sept. 2023, doi: [10.1016/j.ijhydene.2023.07.343](https://doi.org/10.1016/j.ijhydene.2023.07.343).
- [8] J.-F. Dufault, I. E. Achouri, N. Abatzoglou, N. Baridy, L. G. Fréchette, et M. Picard, « Fabrication and Demonstration of Planar Micro-Reactors for Solar Steam Methane Reforming », in *Journal of Physics: Conference Series*, juill. 2018, p. 012055. doi: [10.1088/1742-6596/1052/1/012055](https://doi.org/10.1088/1742-6596/1052/1/012055).
- [9] D. Francoeur et al., « Solar Methane Reforming Microreactor Proof-Of-Concept With A 2X2 Array on a Full-Scale Dish », in *SolarPACES Conference Proceedings*, 2022. Consulté le: 2 mai 2024. [En ligne]. Disponible sur: <https://www.tib-op.org/ojs/index.php/solarpaces/article/view/886>
- [10] J. Bremer et K. Sundmacher, « Operation range extension via hot-spot control for catalytic CO₂ methanation reactors », *React. Chem. Eng.*, vol. 4, n° 6, p. 1019-1037, mai 2019, doi: [10.1039/C9RE00147F](https://doi.org/10.1039/C9RE00147F).
- [11] A. Arman, F. Y. Hagos, A. A. Abdullah, R. Mamat, A. R. A. Aziz, et C. K. Cheng, « Syngas production through steam and CO₂ reforming of methane over Ni-based catalyst-A Review », *IOP Conf. Ser.: Mater. Sci. Eng.*, vol. 736, n° 4, p. 042032, janv. 2020, doi: [10.1088/1757-899X/736/4/042032](https://doi.org/10.1088/1757-899X/736/4/042032).
- [12] Y. Kathiraser, U. Oemar, E. T. Saw, Z. Li, et S. Kawi, « Kinetic and mechanistic aspects for CO₂ reforming of methane over Ni based catalysts », *Chemical Engineering Journal*, vol. 278, p. 62-78, oct. 2015, doi: [10.1016/j.cej.2014.11.143](https://doi.org/10.1016/j.cej.2014.11.143).
- [13] S. A. Paripatyadar, « Cyclic operation of sodium heat-pipe, solar reformers », Ph. D. Dissertation, Univ. of Houston, Houston, TX, United States, 1987. [En ligne]. Disponible sur: <https://www.osti.gov/biblio/5079795>
- [14] J. T. Richardson et S. A. Paripatyadar, « Carbon dioxide reforming of methane with supported rhodium », *Applied Catalysis*, vol. 61, n° 1, p. 293-309, mai 1990, doi: [10.1016/S0166-9834\(00\)82152-1](https://doi.org/10.1016/S0166-9834(00)82152-1).
- [15] Y. Benguerba, L. Dehimi, M. Virginie, C. Dumas, et B. Ernst, « Modelling of methane dry reforming over Ni/Al₂O₃ catalyst in a fixed-bed catalytic reactor », *Reac Kinet Mech Cat*, vol. 114, n° 1, p. 109-119, févr. 2015, doi: [10.1007/s11144-014-0772-5](https://doi.org/10.1007/s11144-014-0772-5).